J Braz. Soc. Mech. Sci. Eng. (2017) 39:3837–3848
DOI 10.1007/s40430-017-0853-2

TECHNICAL PAPER

Vibration monitoring, fault detection, and bearings replacement of a real wind turbine

Henrique D. M. de Azevedo[1] · Pedro H. C. de Arruda Filho[1] · Alex M. Araújo[1] · Nadège Bouchonneau[1] · Janardan S. Rohatgi[1] · Ricardo M. C. de Souza[2]

Received: 27 March 2017 / Accepted: 6 July 2017 / Published online: 18 July 2017

Abstract Wind turbines are growing rapidly in size and diameter. Nowadays, most wind turbines being installed are around 100 m in height and 80–120 m in diameter. Another important characteristic of wind farms is that they are usually far from urban centers. These peculiarities play an important role when analyzing the operation and maintenance costs and its impact in the wind farm project. In remote centers, it becomes crucial to predict and prevent unnecessary maintenance breakdowns and costs. An efficient solution to prevent faults on wind turbines is through condition monitoring. Faults could be prevented by analyzing data from sensors placed around the wind turbines to measure mainly oil quality, temperature, and vibration. In this paper, accelerometers were placed on the main components of a real wind turbine and a vibration-based condition monitoring methodology was applied using signal processing techniques such as Fourier transform, and envelope analysis with Hilbert transform. A bearing fault was discovered and the vibration characteristics were analyzed before and after the bearing replacement.

Keywords Instrumentation and measurements · Vibration monitoring · Fault detection and analyses · Bearing replacement · Wind farm

Technical Editor: Kátia Lucchesi Cavalca Dedini.

✉ Alex M. Araújo
ama@ufpe.br

[1] Department of Mechanical Engineering/Fluid Laboratory, Federal University of Pernambuco, Recife, Brazil

[2] Department of Electronics and Systems, Federal University of Pernambuco, Recife, Brazil

1 Introduction

With increasing public awareness of the unsustainability of traditional fossil fuels and its severe effects on the environment, renewable energy gains more and more share in the total energy consumption [1]. Therefore, wind power is rapidly developing in almost every part of the world. The statistics from the Global Wind Energy Council informs that, in the period 1996–2011, the medium rate of increase of worldwide wind power installation was higher than 20%, and by the end of 2011, the capacity was of the order 240 GW [2]. Almost 52 GW of wind power was installed in 2014, bringing the total installed global capacity to more than 369.6 GW at the end of 2014 [3]. In 2015, 2.75 GW were installed in Brazil, a record, bringing the total to 8.72 GW, which accounts for 6.3% of the Brazilian energy matrix [4].

The above wind energy capacity was possible due to installation of wind turbines with more than 2 MW. These turbines have rotor diameter above 80 m and as such require high precision built parts and components. Small faults/defects can become big problems for wind farm operators, mainly for those in remote areas where it is difficult to access machinery and spare parts. Therefore, it is imperative to use condition monitoring to prevent and predict faults before they actually impact the production [5]. In addition, it is important to mention that wind turbines operate in very severe and variable environmental conditions as compared to other traditional power generation systems. Wind turbines (WT) are subjected to rapid change of temperature, pressure, solar insolation, rain, hail, and storms, etc. Due to these external variants, WT are subjected to varying dynamic loads resulting into increased vibrations [6, 7].

The basic configuration of a typical commercial WT has a rotor mounted on a slow rotating shaft supported on bearings. The slow motion of this shaft called main shaft is connected to a gearbox with two-to-three stages, so that the desired rotation of the order of 1200–1800 rpm is available to the generator. The shaft at every stage of the gearbox is also supported on bearings and so is the generator shaft. Figure 1 shows a schematic of a WT and the sensors installed on the bearings as per our methodology proposed in this work.

Wind energy, a renewable source of energy, is growing at a fast pace in the world. However, unpredictable failure of certain wind turbine components, (such as turbine blades, tower, gearbox, generator, braking system, and yaw system), can lead to substantially higher maintenance costs and reduced availability of wind turbines [9]. Therefore, the nascent wind industry suffers with a premature breakdown of principal turbine components, leading to an increase of operation and maintenance (O&M) costs, thereby increasing the cost of energy generated [2].

In paper [6] the authors showed that the rate of turbine breakdowns for large-sized turbines (>1000 kW) is higher than the small/medium-sized (225–1000 kW) turbines. Since modern wind turbines tend to grow in size, the reduction of O&M costs, especially for large turbines, is of utmost importance, and this would result into increased reliability and confidence. The need of wind turbine condition monitoring and its advantages can be exemplified by the growth in the numbers of publications. For example, in 2005, there were only about 30 publications on condition monitoring of WTs and it increased exponentially to almost 140 in 2013 [10–12].

The breakdown of principal components causes greater financial impact due to unexpected maintenance and downtimes. It has been reported by the National Renewable Research Laboratory that the breakdowns due to gearbox, electrical systems, rotor, and generator take up almost 70% time of the downtime [13]. However, it is essential to understand the impact of sub-components such as bearings of these faults [14, 15]. Various publications on condition monitoring focus on gearbox and generators because of financial impact, fault frequency, and high downtime.

A number of papers employ Supervisory Control and Data Acquisition (SCADA) for condition monitoring but does not use vibration measurements of bearing at high frequency [16, 17]. However, bearings are the root cause of failure of gearboxes and generator; they cause around 70% of faults on gearboxes and 21–70% of faults on generators [13]. This is the principal justification to use predictive maintenance of bearings based on condition monitoring. The Figs. 2, 3 and 4 below show the different reasons of gearbox breakdown, the number of substitutions of gearbox (GBX) and generators (GEN) over time and the downtime for gearbox (GBX) and medium generators—1 to 2 MW (GEN).

Hence, this paper aims to present a full-scale real case of wind turbine monitoring in the Brazilian northeast applying the methodology for condition monitoring of bearing based on the analysis of temporal vibration signals, fast Fourier transformation (FFT), and envelope analysis by Hilbert transformation.

This paper is structured as follows: Sect. 2 introduces the method proposed, Sect. 3 describes case study, and Sect. 4 presents results and discussions, and finally, Sect. 5 provides conclusions.

2 Proposed methodology

The application of the proposed method requires accelerometers to be placed on the main components of the wind turbine. The data are compared to an international standard: VDI-3834, specifically, developed for WTs [20].

The raw vibration data are analyzed by three independent techniques: time domain analysis, spectral analysis (by fast Fourier transformation), and envelope analysis (by Hilbert transformation). A brief account of these

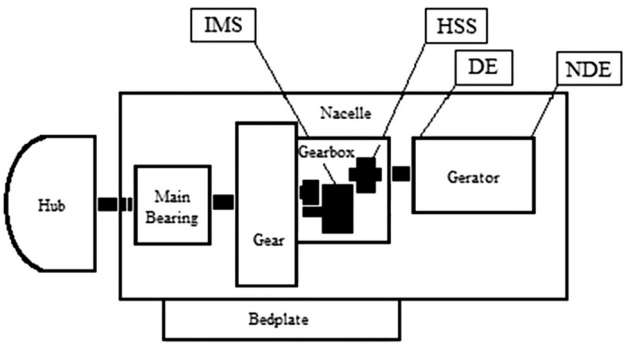

Fig. 1 Layout of a typical wind turbine and location of sensors: intermediate Shaft (IMS), high-speed shaft (HSS), drive end (DE), and non-drive end (NDE). Adapted from [8]

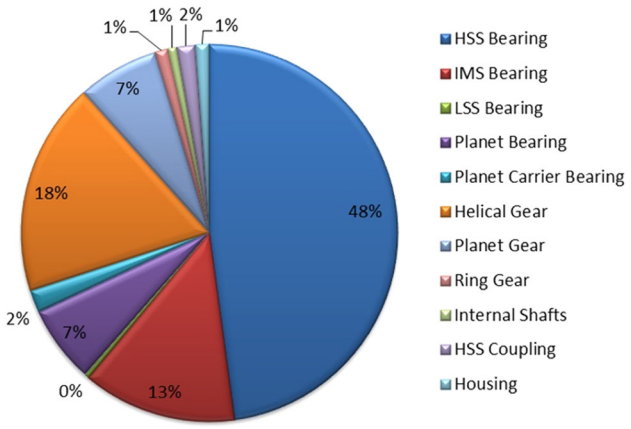

Fig. 2 Different reasons of gearbox breakdown and their %. Adapted from [13]

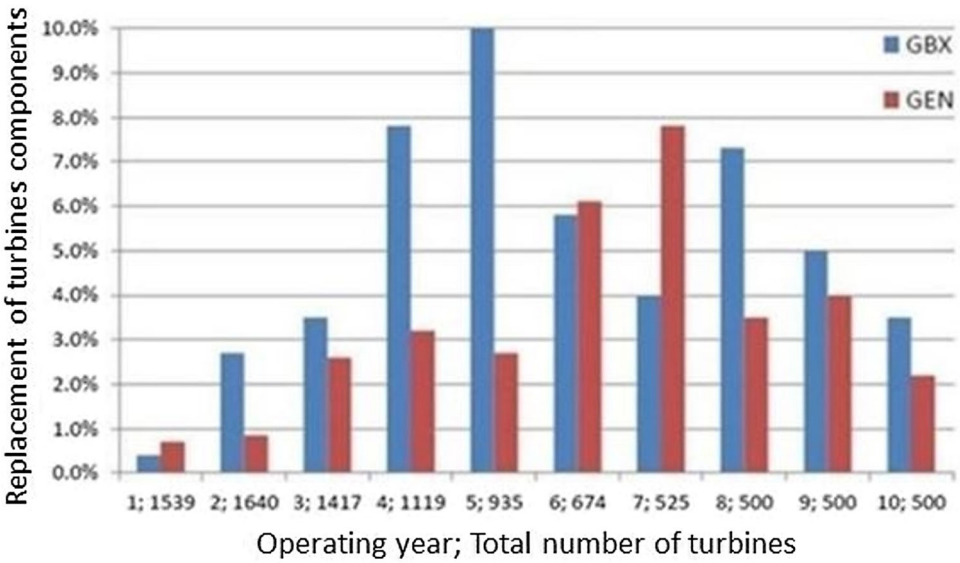

Fig. 3 Substitutions of gearbox (GBX) and generators (GEN). Adapted from [18]

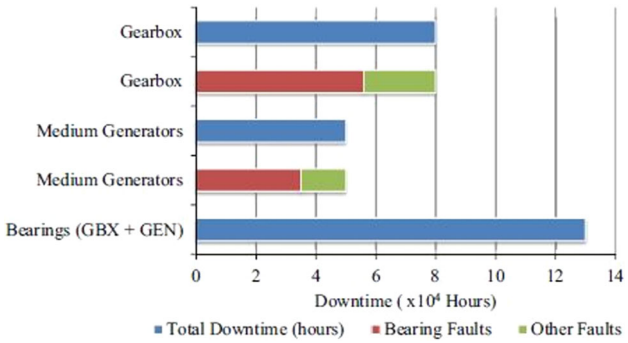

Fig. 4 Downtime for gearbox (GBX) and medium generators—1 to 2 MW (GEN). Adapted from [13, 19]

techniques is discussed in Sect. 3.3. The three techniques are applied independently and later on are analyzed jointly. The order of their application does not interfere in the final outcome, because the three techniques are not dependent on each other. Usually, a critical fault is detected by all the three analyses. At times, only one of the techniques is sufficient to identify a fault. A flowchart, Fig. 5, illustrates the methodology used in this paper.

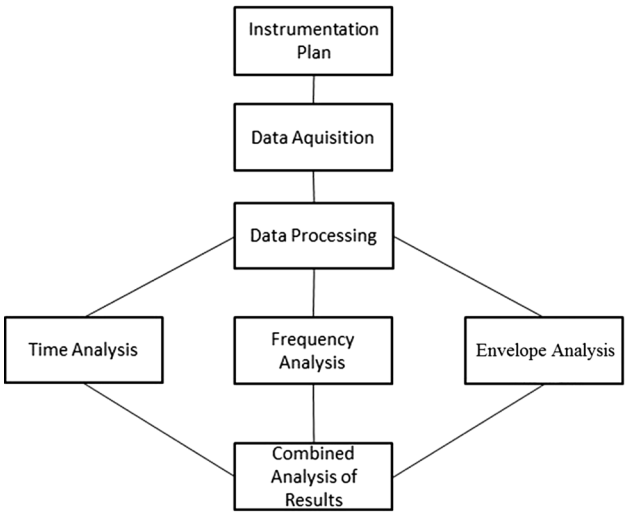

Fig. 5 Schematic of proposed methodology

3 Case study

The study was carried out on a specific WT in a windfarm in Brazil. To identify possible fault(s) in the WT, the vibration signals were measured from June 1 to September 30, 2014.

3.1 Instrumentation of a wind turbine

Accelerometers are placed in the main components of wind turbine; these sensors are mostly based on the piezoelectric principle, in which a change in pressure is converted to an electric signal. The acceleration acts upon a seismic mass (a crystal) that is restrained by a spring and converts a physical force into an electrical signal. The measurement of acceleration is highly dependent on the method on which these are mounted on the surface under test. To obtain precise measurements, the sensors have to be attached firmly to the surface that is being tested.

Figure 6 shows the locations of accelerometers and tachometer in the wind turbine. The sensors are connected to a datalogger that is connected to a switch. The wind turbine system can be classified into two distinct regions: low frequency (consisting of rotor assembly, main shaft, and first stage of the gearbox), and of high frequency (consisting of second and third stages of the gearbox) and generator. The speed of the main shaft bearing and the input shaft of the

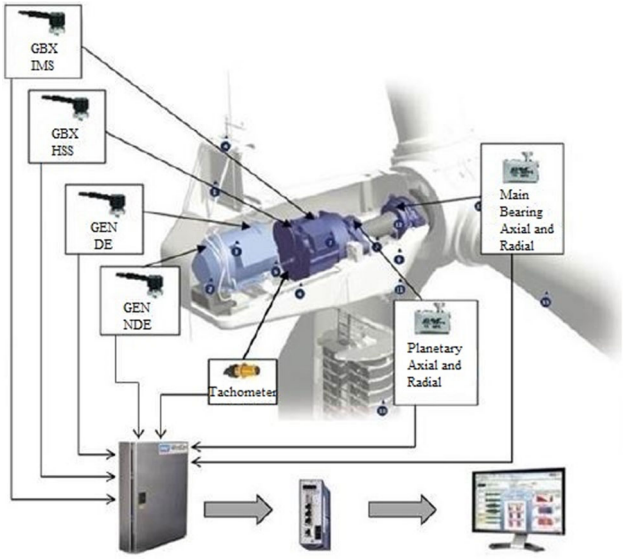

Fig. 6 Location of sensors in turbine. Adapted from [26]

gearbox bearing runs at a slower speed; therefore, higher precision accelerometers are required in these locations. On the other hand, accelerometers of high frequencies are required for intermediate shaft (IMS), high-speed shaft of the gearbox (HSS), and on the both ends of the generator: drive end (DE) and non-drive end (NDE). The sensors for low and high frequencies are commercially available [21, 22].

All the sensors were connected to a datalogger [23]. The datalogger was affixed on the panel in the nacelle vertically and far away from the sensors to avoid influence of vibrations. The commutators or switches connect the datalogger to a central control command, located preferably at the bottom of the tower [24]. Lastly, the tachometer is installed in between the gearbox and the generator [25]. The signals from the sensors are stored in the datalogger.

3.2 International standards for vibration analyses

The international standard ISO 10816-3 is applicable to rotating machines which primarily deals with the mechanical vibrations in the steam turbines, generators of varying sizes, and general industrial machines. However, WT works under very variable conditions and as such ISO standard cannot be used. For example, vibrations of the tower and nacelle of a WT caused by the effects of wind, flow disturbances due to tower shadow, and the natural vibrations of the blades, and tower makes ISO standard not applicable to the WTs. This standard is not specific for wind turbines. In addition, due to flexibility of blades and tower, there is a necessity to include low-frequency vibrations in any standard for WT. As a result, the association of German Engineers VDI (in German: Verein Deutscher Ingenieure) in collaboration with turbine manufacturers and users developed the standard VDI-3834 [18] for WT. This standard enables to assist in the evaluation of vibrations in a WT and its components. Table 1 shows the VDI-3834 standard where the magnitude of the acceleration for different elements of a WT is listed. The standard establishes three levels of vibrations. Level I represents vibrations which are considered normal; level II indicates that the vibrations are abnormal for continued operation and also suggests that further analyses should be done to identify the reason(s) of possible fault(s). Whereas vibrations of level III are considered dangerous and may lead to significant damage to WT and its components.

In case of gearboxes, there is usually a slow speed shaft, an intermediate shaft, and a high-speed shaft. As such, the frequencies of these shafts (or bearings on which these are supported) are divided into $\leq$0.1 to 10 Hz and >10 to 2000 Hz. The values of acceleration are estimated from the individual measurements and converted into a root-mean-squared (rms) value.

3.3 A short note on the techniques

The following subsections provide a brief account of the three techniques used in this paper.

3.3.1 Time domain vibration signals

The vibrations measured by displacement are called time waveforms or temporal vibrations. The amplitude of the signal represents the amount of displacement. By measuring the displacement and differentiating, one obtains the velocity and the acceleration. The signal is composed of sinusoids, expressed as follows:

$$x(t) = A \sin(\omega t + \phi), \tag{1}$$

where A = vibrational amplitude; ω = angular frequency of oscillation; and ϕ = phase of the waveform. Then, the velocity $v(t)$ and acceleration $a(t)$ are defined as:

$$v(t) = A\,\omega \cos(\omega t + \phi), \tag{2}$$

$$a(t) = -A\,\omega^2 \sin(\omega t + \phi). \tag{3}$$

The temporal variations could be either periodic or random; and at times they could also be transitional, which usually disappear with time. The analysis of temporal variations is rather difficult, because there could be excitations of the element, and as such, they are complex at times to analyze [27].

3.3.2 Spectral analysis (FFT)

An easier and better way to analyze the vibration signals is by measuring its frequency spectrum. This is done by the

Table 1 Level of severity by VDI standard [20]

Component	Frequency range (Hz)	Level	Acceleration in rms
Nacelle and Tower	0.1–10	I/II	0.3
		II/III	0.5
Rotor shaft bearing	0.1–10	I/II	0.3
		II/III	0.5
Gearbox bearing	0.1–10	I/II	0.3
		II/III	0.5
	10–2000	I/II	7.5
		II/III	12.0
Generator shaft bearing	10–5000	I/II	10
		II/III	16

Table 2 Results of vibration level: intermediate shaft (IMS), high-speed shaft (HSS), drive end (DE), and non-drive end (NDE)

Location	Jun (VDI Level)	Jul (VDI Level)	Aug (VDI Level)	Sep (VDI Level)
IMS (0.1–10 Hz)	1.55 (I/II)	1.22 (I/II)	0.67 (I/II)	1.02 (I/II)
HSS (10–2000 Hz)	4.85 (I/II)	4.46 (I/II)	5.12 (I/II)	2.99 (I/II)
DE	6.82 (I/II))	10.54 (II/III)	7.14 (I and II)	7.98 (I/II)
NDE	12.44 (II/III)	12.32 (II/III)	14.09 (II/III)	13.45 (II/III)

fast Fourier transform (FFT) algorithm. The advantage of frequency domain analysis over temporal analysis is its ability to identify and isolate certain frequency components of interest. All bearing elements generate vibration at specific frequencies, referred to as fault frequencies, and they can be calculated according to the bearings structure and dimensions. Thus, the vibration spectrum is an efficient tool in the detection of frequencies of failures of a bearing. However, many times, the peaks of frequencies of failures in the bearing are close to the peak of the vibrating noise signal (mostly in the early wear phase of the bearing) [27–29].

3.3.3 Envelope analysis (Hilbert transformation)

Another very effective technique for detecting and predicting bearing failure is the analysis of the signals resulting from demodulation of high-frequency vibrations, emitted by defective bearings; it is called envelope analysis of vibrations [6]. This approach can extract very low-amplitude and low-frequency periodic signals that might be masked by other higher energy vibrations as in the gearboxes [30, 31]. While the raw spectrum can be useful for monitoring gear mesh frequencies, the envelope spectrum provides superior sensitivity to bearing defect frequencies in WT applications [32]. With its high sensitivity, demodulation has been proven to be good for evaluating defects that produce impacting, e.g., rolling contacts in bearings and tooth-to-tooth contacts in the gear meshes [33]. It also helps to reduce the complexity of the analysis, the main advantage being that it provides excellent visibility of bearing defects in an early stage without the interference of gear mesh frequencies in the same spectrum.

4 Results and discussions

The following subsections analyze the vibration signals monitored on a WT [26].

4.1 Data processing and analysis by the VDI-3834 standard

A summary of the vibration measurements for each month and location is shown in Table 2. It shows that the vibrations for IMS are the least and increases from HSS to DE to NDE. For example, all the accelerations of IMS were less than the standard value of 7.5 m/s^2. Therefore, it can be stated that the IMS of the gearbox bearing is running under normal condition (between Level I and Level II). Similarly, the bearing of the HSS has vibration level between I and II (i.e., below the standard value of 7.5); therefore, it may be concluded that this bearing is also running under normal conditions.

Analyzing the generator at the DE location, it is seen that most of the vibrations are in between Level I and Level II, because the VDI standard value of vibration for generator is less than 10 m/s^2. Though, in the month of July, a vibration of 10.54 (very close to the standard value) was measured and thus indicates some abnormality in the bearing. However, in the following months, it was noted

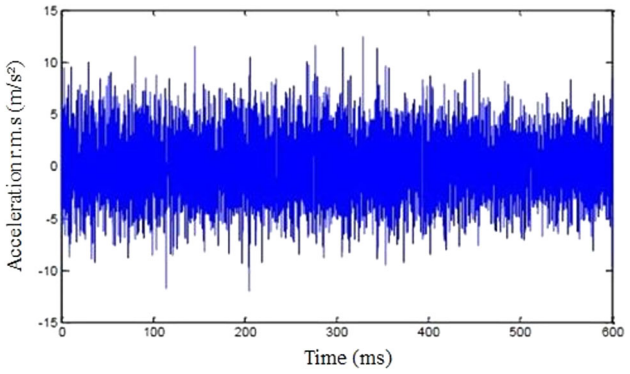

Fig. 7 Plot of temporal signal: HSS

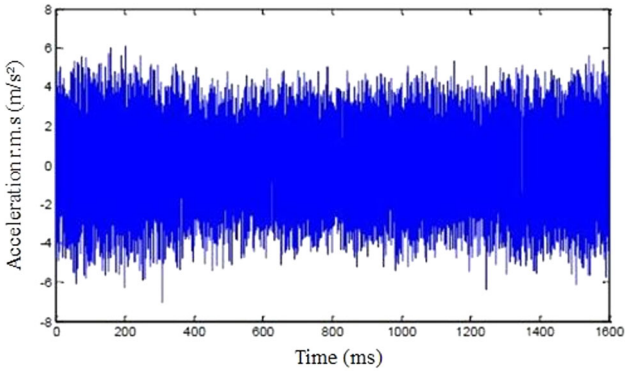

Fig. 8 Plot of temporal signal: IMS

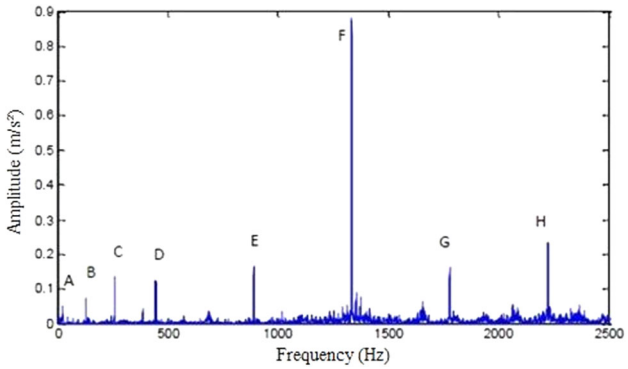

Fig. 9 Spectrum plot: IMS

that it was actually being cause by the NDE fault identified later. Therefore, it can be said that the DE side of the generator bearing is running normal.

Finally, analyzing the NDE location, the vibration for any month is higher than 10 but less than 16 m/s^2, indicating that the bearing is running beyond normal level and attention is required to look into the reason of fault in it. The following sections describe for the month of September 2014, the analyses for the gearbox and the generator.

4.2 Analysis of gearbox

For the analysis of gearbox, Figs. 7, 8 show the temporal variation of the accelerometer mounted on the high-speed shaft (HSS), and on the intermediate shaft (IMS), respectively. These plots indicate that most of the peaks are of low amplitudes (less than 10 m/s^2); the spikes represent regular gear meshing frequencies and do not reveal any significant defect.

Figure 9 shows the spectral plot for the IMS, where peaks are marked: A through H. These peaks are analyzed in Table 3. The harmonic peaks are estimated, where peak A is the first harmonic of the second stage of the gearbox, and peaks B and C are its second and third harmonics. Similarly, peaks D through H are for the third stage of the gearbox, where D is the first harmonic, and E, F, G, and H are its harmonics. These peaks are generated due to gear meshing and they are always present, since the amplitudes are relatively low compared to the VDI standard and they did not show any vibration growth over the analyzed period which they can be considered normal.

Figure 10 shows plots of spectral analyses for HSS, three peaks are marked at an interval of about 500 Hz. Table 4 analyzes these peaks. Peak A is the first harmonic of the third stage of the gearbox, and peaks B and C are its harmonics.

Figure 11 shows the plot of envelope for the IMS bearing, indicating a peak A. This peak was estimated at about 440 Hz, first harmonic of the second stage of the gearbox. Plot of envelope reveals one peak A, which is the first harmonic of the third stage of the IMS. This envelope does not present a significant frequency as its amplitude is less than 0.4 m/s^2, see Table 1.

Figure 12 shows the plot of envelope of HSS, indicating an acceleration of less than 0.6 m/s^2. This frequency is caused by the gear meshing and considering its low amplitude and does not grow with time; it may be concluded that the envelope plots does not show any significant frequency, see Table 1.

Therefore, the analyses of the gearbox by spectral and envelope techniques indicate that there is no significant defect in it.

4.3 Analysis of generator

The analyses of the bearings for the generator were done at both ends of its shaft: drive end (DE) and non-drive end (NDE). Figures 13, 14 show plots of temporal vibrations of the generator shaft, revealing higher acceleration for the NDE compared to the DE. Figure 15 is a zoom of Fig. 14 and two peaks (A and B) are marked on it. The time interval between the peaks A and B is 9.45 ms (=16.02 − 6.57), resulting into a frequency (inverse of

Table 3 Frequencies of interest shown in Fig. 9

Points	Comments
A	First harmonic of the meshing frequency of the second stage of the gearbox
B	Second harmonic of the meshing frequency of the second stage of the gearbox
C	Third harmonic of the meshing frequency of the second stage of the gearbox
D	First harmonic of the meshing frequency of the third stage of the gearbox
E	Second harmonic of the meshing frequency of the third stage of the gearbox
F	Third harmonic of the meshing frequency of the third stage of the gearbox
G	Fourth harmonic of the meshing frequency of the third stage of the gearbox
H	Fifth harmonic of the meshing frequency of the third stage of the gearbox

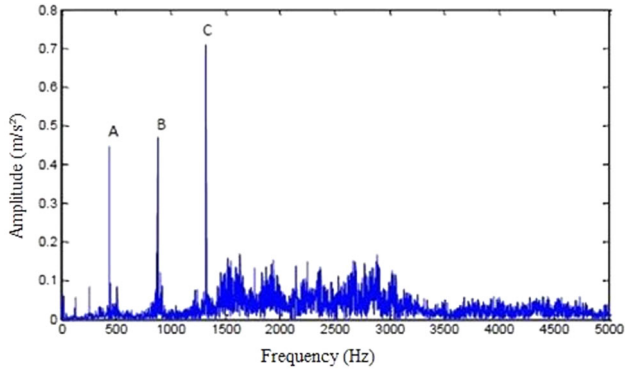

Fig. 10 Spectrum plot: HSS

Table 4 Frequencies of interest shown in Fig. 10

Points	Comments
A	First harmonic of the meshing frequency of the third stage of the gearbox
B	Second harmonic of the meshing frequency of the third stage of the gearbox
C	Third harmonic of the meshing frequency of the third stage of the gearbox

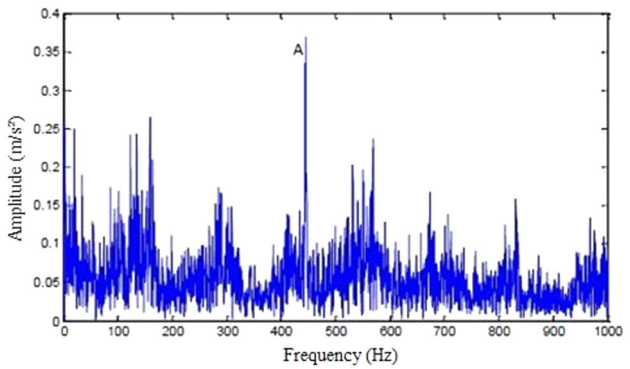

Fig. 11 Plot of envelope: IMS

9.45 ms) of 105.8 Hz, rounded to 106 Hz. It was calculated and found that this number represents the frequency of an inner race fault on the NDE bearing.

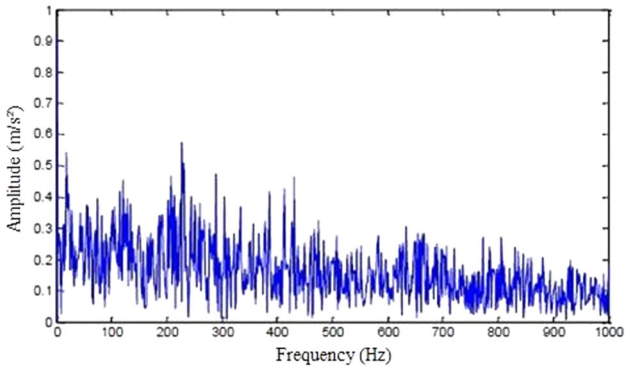

Fig. 12 Plot of envelope: HSS

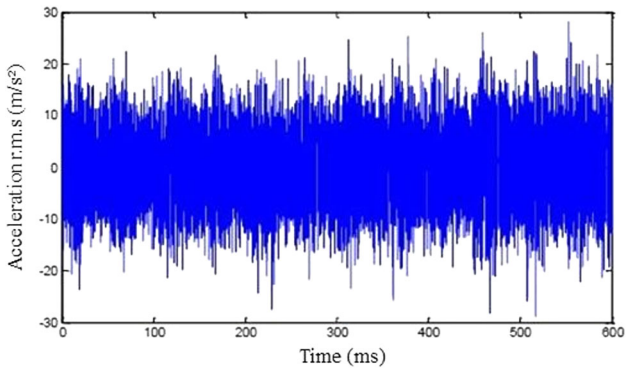

Fig. 13 Plot of temporal signal: DE

Figure 16 shows the spectrum plot of the generator shaft at the DE. Table 5 shows the analyses of the peaks of these figures. It was calculated that peak A is the first harmonic of the third stage of the gearbox and peak C is due to the third harmonic of the third stage of the gearbox.

Figure 17 shows the spectrum plot at the NDE, and in Table 6, the peaks A–D are shown. It was estimated that peak D is due to the bearing resonance. What is of interest is that peaks for the DE (in Fig. 16) are repeated in Fig. 17 (labeled A and C). However, this is due to the passing of the frequencies of the gearbox to the generator. These peaks contain a large amount of energy because of gear

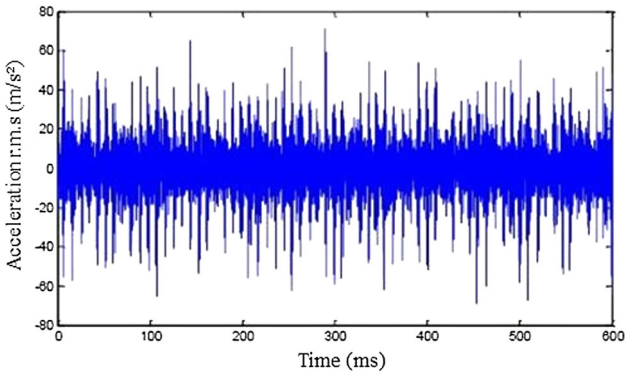

Fig. 14 Plot of temporal signal: NDE

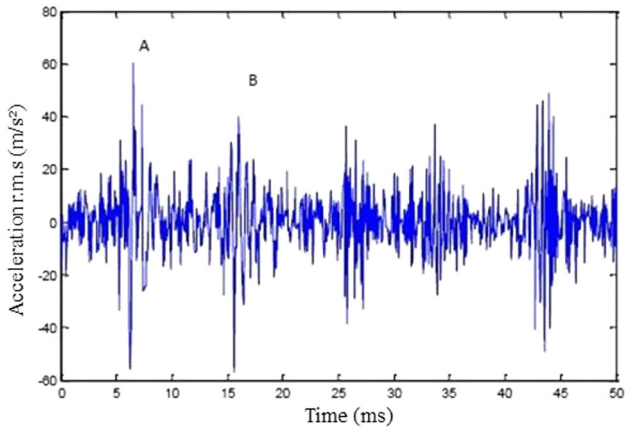

Fig. 15 Enlarged plot of temporal signal: NDE

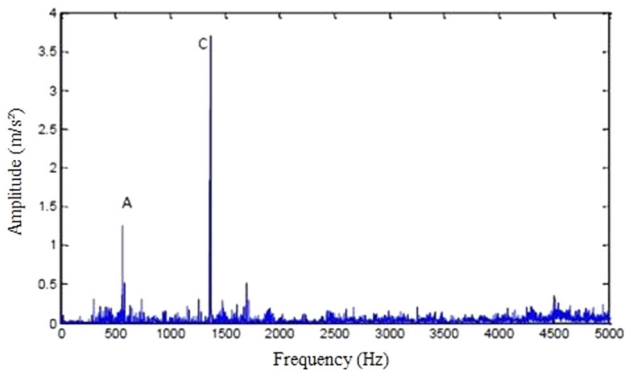

Fig. 16 Spectrum plot: DE

Table 5 Frequencies of interest shown in Fig. 16

Points	Comments
A	First harmonic of the meshing frequency of the third stage of the gear box
C	Third harmonic of the meshing frequency of the third stage of the gear box

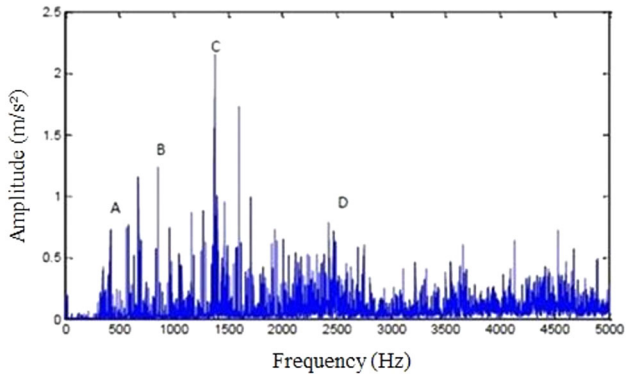

Fig. 17 Spectrum plot: NDE

meshing and natural impact that does occur in the HSS of the gearbox.

The spectrum at the NDE is further zoomed from 5000 to 300 Hz, Fig. 18. The peaks A, B, and C are analyzed in Table 7, where the peak A is clearly the frequency of the HSS; peak B (frequency of about 120 Hz) is associated with the BPFI (Ball Pass Frequency of the Inner race) of the generator at the NDE; and peak C is approximately the second harmonic corresponding to 2×BPFI. Therefore, it indicates a fault in the inner raceway of the bearing.

Figure 19 shows the plot of envelope for the DE. Table 8 shows the peaks marked in Fig. 19. For example, peak A is the speed of the HSS of the gearbox at the DE, whereas peak B is the frequency of the defect in the inner race of the bearing (BPFI), and D and F are its multiples. The peaks C and E are the first and the second harmonics of the IMS shaft (second stage) of the gearbox, respectively. It is seen that the amplitudes of these peaks are low (<2 m/s^2).

Figure 20 shows a plot of the envelope for the NDE, indicating clearly three peaks: A, B, and C at about 20, 106, and 212 Hz, respectively. Table 9 shows these peaks and their origin. This plot identifies peaks at about 20 Hz (representing the frequency of the HSS) and at 106 Hz (indicating BPFI at the NDE of the generator where the amplitude of acceleration is of the order of 12 m/s^2. The estimation (of frequency of 106 Hz) was attributed to a fault in the inner race of the bearing. It is also seen in Fig. 19 that the amplitudes of the DE are quite small (order of 2 m/s^2) compared to that of NDE (>10 m/s^2).

Figures 21, 22, 23, 24 [34] show the faults in the bearing at four stages (Stage 1 through Stage 4). It can be seen that Stage 3 (Fig. 23) and Stage 4 (Fig. 24) match well with the fault revealed in the NDE of the generator. This further confirms that there is a defect in this bearing NDE.

Table 6 Frequencies of interest shown in Fig. 17

Points	Comments
A	First harmonic of the meshing frequency of the third stage of the gearbox
B	Second harmonic of the meshing frequency of the third stage of the gearbox
C	Third harmonic of the meshing frequency of the third stage of the gearbox
D	Peaks in the bearing resonance frequencies

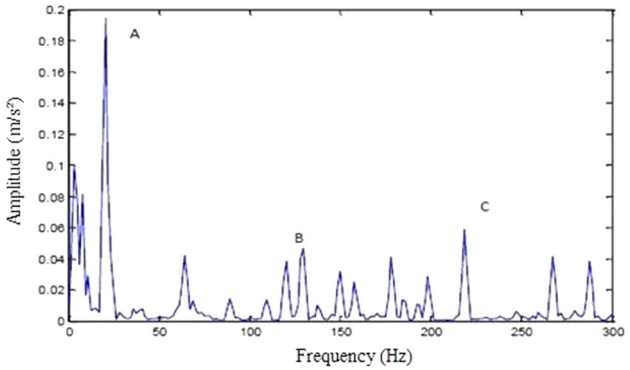

Fig. 18 Enlarged Spectrum plot: NDE

Table 7 Frequencies of interest shown in Fig. 18

Points	Comments
A	Frequency of HSS
B	Frequency of approximately 106 Hz linked to BPFI of bearing
C	Frequency of approximately 212 Hz linked to 2×BPFI of bearing

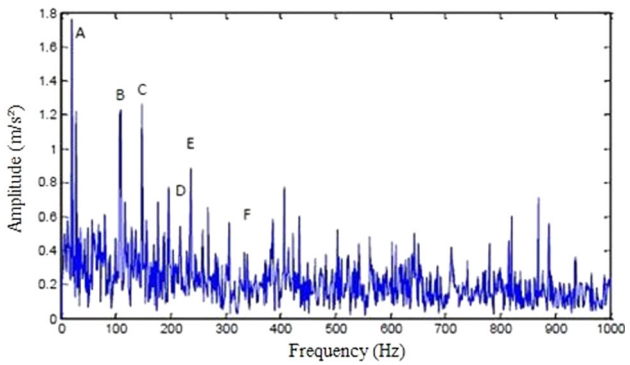

Fig. 19 Plot of envelope: DE

4.4 Analyses after fault detection

It has been established that the bearing on the non-drive end of the generator is faulty. Therefore, it was replaced on 14 October, 2014, and it took almost 15 h to do it.

Figure 25 shows that after the substitution of the bearing, the value of temporal acceleration dropped from about 12 m/s^2 to less than 5 m/s^2 as shown by the red color. The temporal variation after the replacement of the bearing also improved, see Fig. 26. Not only this, the temporal variation of the generator at the DE also improved considerably (Fig. 27).

Table 8 Frequencies of interest shown in Fig. 19

Points	Comments
A	Frequency of HSS
B	Frequency of approximately 106 Hz linked to BPFI of bearing
C	First harmonic of the meshing frequency of the second stage of the gearbox
D	Frequency of approximately 212 Hz linked to 2×BPFI of bearing
E	Second harmonic of the meshing frequency of the second stage of the gearbox
F	Frequency of approximately 318 Hz linked to 3×BPFI of bearing

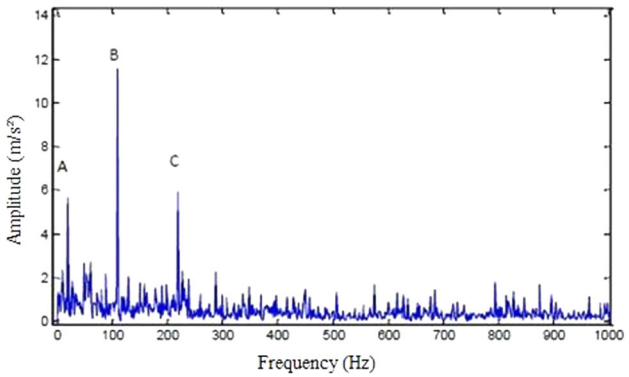

Fig. 20 Plot of envelope: NDE

Table 9 Frequencies of interest shown in Fig. 20

Points	Comments
A	Frequency of HSS
B	Frequency of approximately 106 Hz linked to 2×BPFI of bearing
C	Frequency of approximately 212 Hz linked to 2×BPFI of bearing

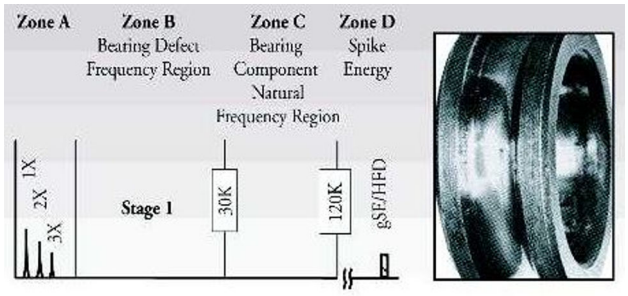

Fig. 21 Spectrum of a bearing failure in the first stage

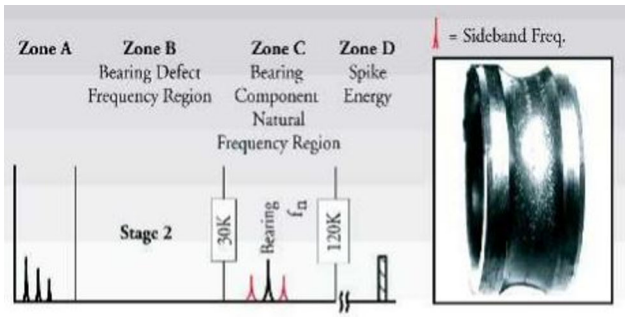

Fig. 22 Spectrum of a bearing failure in the second stage

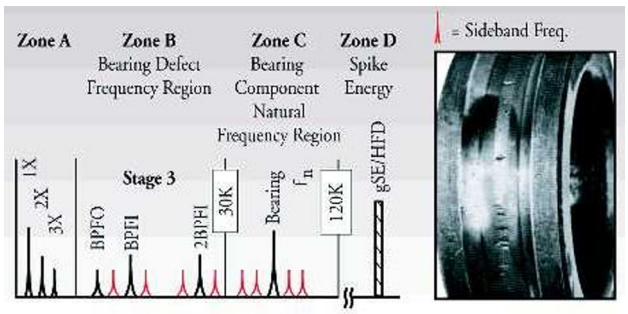

Fig. 23 Spectrum of a bearing failure in the third stage

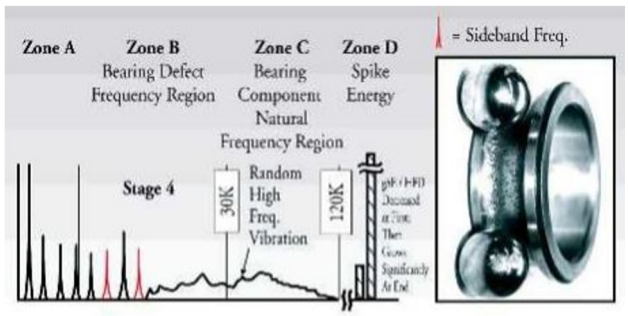

Fig. 24 Spectrum of a bearing failure in the fourth stage

Similarly, the spectral plots of the NDE and DE show a remarkable reduction of acceleration amplitudes (Figs. 28 and 29), indicating the influence of the replaced bearing.

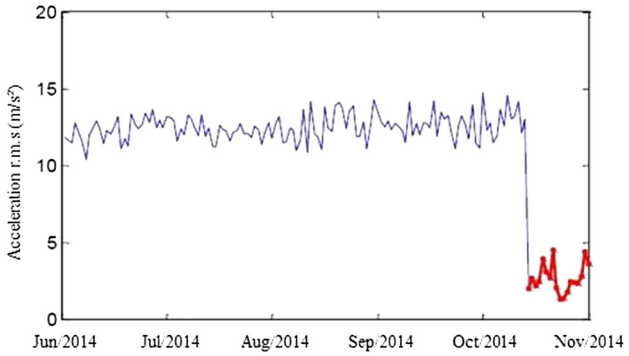

Fig. 25 Comparison with the VDI 3834 standard after replacing the bearing on the NDE side

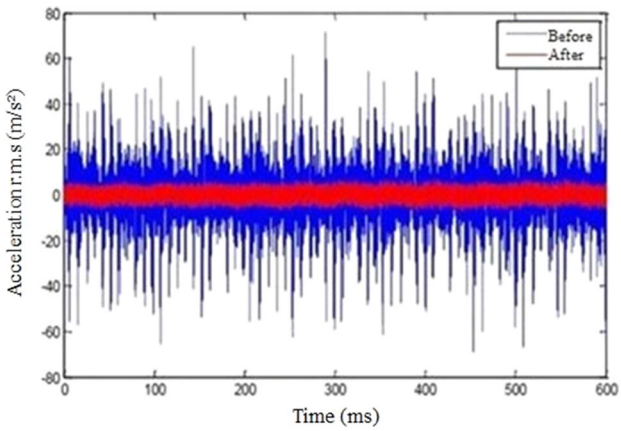

Fig. 26 Comparison of the temporal signal on the NDE side: before and after the bearing replacement

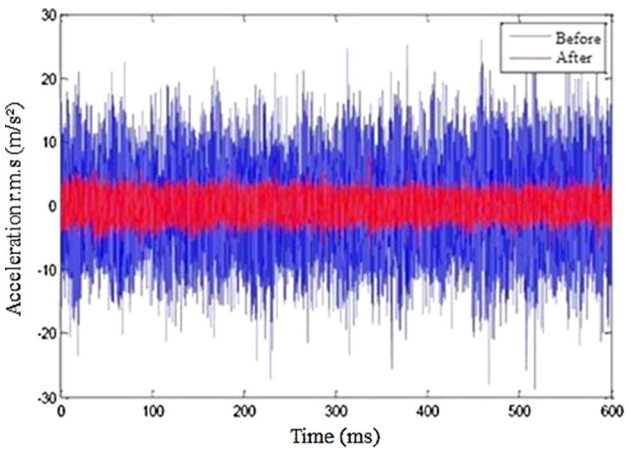

Fig. 27 Comparison of the temporal signal on the DE side: before and after the bearing replacement

The envelop plot of the NDE (Fig. 30) shows very significant improvement. For example, at the frequency of approximately 106 Hz, the amplitude was about 12 m/s^2, before changing the bearing, and after it was less than 1 m/s^2. There was a change of amplitude for the DE bearing

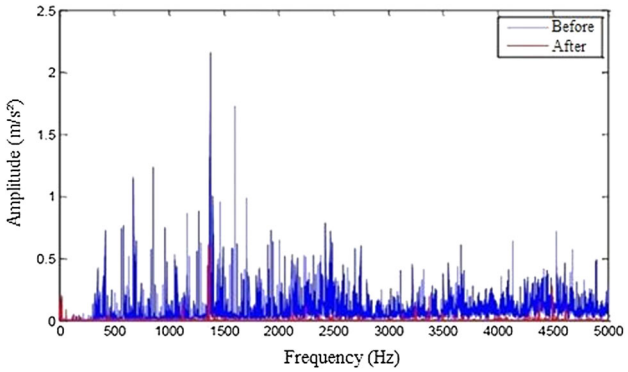

Fig. 28 Comparison of the spectrum on the NDE side: before and after the bearing replacement

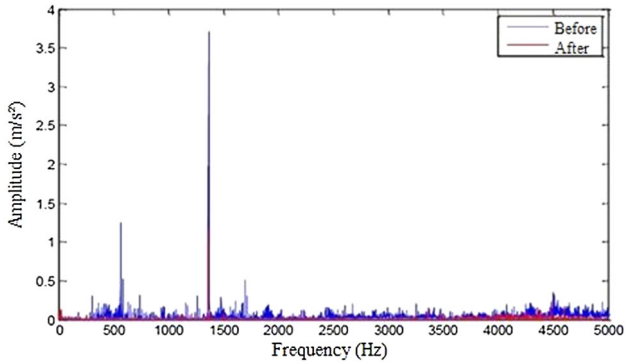

Fig. 29 Comparison of the spectrum on the DE side: before and after the bearing replacement

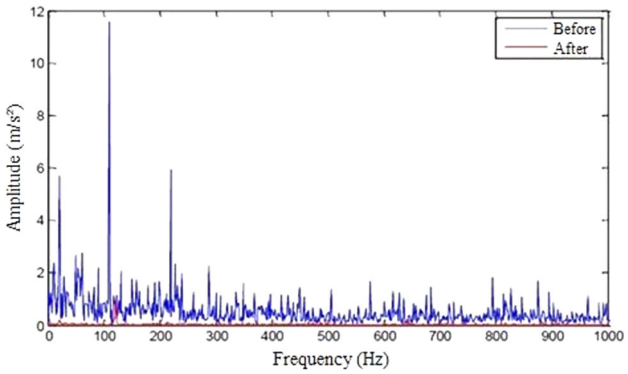

Fig. 30 Comparison of the envelope on the NDE side: before and after the bearing replacement

(Fig. 31) as well, but in comparison to the NDE, it was not significant.

5 Conclusions

In this work, condition monitoring of bearings of the gearbox and generator was monitored by accelerometers. The campaign was run for 4 months. The vibration

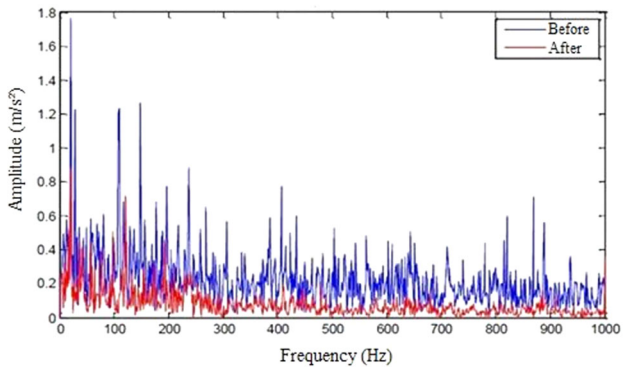

Fig. 31 Comparison of the envelope on the DE side: before and after the bearing replacement

measured was compared to the international standard VDI-3834 specifically created for wind turbines.

Furthermore, the analyses were performed using the proposed methodology in this work that consisted in the application of the three classical analyses: temporal variations of vibrating signals, and spectrum analyses by fast Fourier transforms and envelope analysis through Hilbert transformation.

The results from the analyses assisted in finding a fault in the non-drive end bearing of the generator. The inner race of the bearing was found dented. The bearing was replaced by a new bearing and further monitoring showed that the vibration levels were reduced significantly.

Acknowledgements This work was partly funded by Brazilian research councils Coordenação de Aperfeiçoamento de Pessoal de Nível Superior—CAPES, Conselho Nacional de Desenvolvimento Científico e Tecnológico—CNPq and Pró-Reitoria de Pesquisa e Pós-Graduação—UFPE/PROPESQ.

References

1. Yang J, Yang P (2016) Random vibration and dynamic analysis of a planetary gear train in a wind turbine. Shock Vib. doi:10.1155/2016/6292953
2. Sheng S and Veers P (2011) Wind turbine drivetrain condition monitoring—an overview. In: Mechanical Failures Prevention Group, applied systems health management conference; 2011 May 10–12; Virginia Beach, Virginia. NREL, USA
3. Global Wind Energy Council (2016a) GWEC The international trade association for the wind power industry. http://www.gwec.net/global-figures/wind-in-numbers/. Accessed 27 Mar 2016
4. Global Wind Energy Council (2016b) GWEC The international trade association for the wind power industry. http://www.gwec.net/brazil-windpower-2016/. Accessed 27 Apr 2016
5. Azevedo HDM, Araújo AM, Bouchonneau N (2016) A review of wind turbine bearing condition monitoring: state of the art and challenges. Renew Sustain Energy Rev 56:368–379. doi:10.1016/j.rser.2015.11.032
6. Márquez FP, Tobias AM, Pérez JM, Papaelias M (2012) Condition monitoring of wind turbines: techniques and methods. Renew Energy 46:169–178. doi:10.1016/j.renene.2012.03.003

7. Koulocheris D, Gyparakis G, Stathis A, Costopoulos T (2013) _ Vibration signals and condition monitoring for wind turbines. Engineering 5:948–955. doi:10.4236/eng.2013.512116
8. Zimroz R, Bartekmus W, Barszcz T, Urbanek J (2014) Diagnostics of bearings in presence of strong operating conditions non-stationarity-a procedure of load-dependent features processing with application to wind turbine bearings. Mech Syst Signal Process 46(1):16–27. doi:10.1016/j.ymssp.2013.09.010
9. Romero A, Lage Y, Soua S, Wang B, Gan T-H (2016) Vestas V90-3 MW wind turbine gearbox health assessment using a vibration-based condition monitoring system. Shock Vib. doi:10.1155/2016/6423587
10. Nie M, Wang L (2013) Review of condition monitoring and fault diagnosis technologies for wind turbine gearbox. In: 2nd International Through-life Engineering Services Conference; 2013 November 5–6; Cranfield, Cranfield University, UK. Elsevier, UK, pp 287–290. doi:10.1016/j.procir.2013.07.018
11. He D, Bechhoefe E, Saxena A (2013) Editorial: special issue on wind turbine prognostics and health management. Int J Health Proagnostics 4(2):1–2
12. Tachakoua P, Wamkeue R, Ouhrouche M et al (2014) Wind turbine condition monitoring: state-of-the-art review, new trends, and future challenges. Energies 7(4):2595–2630. doi:10.3390/en7042595
13. Sheng S, Keller J and Glinsky C (2013) Gearbox reliability collaborative update. Sandia Reliability Workshop; 2013 August 13–14; Albuquerque, NM. NREL, USA
14. Xueli A, Dongxiang J, Jie C, Chao L (2011) Application of the intrinsic time-scale decomposition method to fault diagnosis of wind turbine bearing. J Vib Control 18(2):240–245. doi:10.1177/1077546311403185
15. Lin B, Chang P (2016) Fault diagnosis of rolling element bearing using more robust spectral kurtosis and intrinsic time-scale decomposition. J Vib Control 22(12):2921–2937. doi:10.1177/1077546314547727
16. Sun P, Li J, Wang C, Lei X (2016) A generalized model for wind turbine anomaly identification based on SCADA data. Appl Energy 168:550–567. doi:10.1016/j.apenergy.2016.01.133
17. Astolfi D, Castellani F, Garinei A, Terzi L (2015) Data mining techniques for performance analysis of onshore wind farms. Appl Energy 148:220–233. doi:10.1016/j.apenergy.2015.03.075
18. Sheng S (2013) Report on wind turbine subsystem reliability—a survey of various database. Report. National Renewable Energy Laboratory (USA)
19. Whittle M (2015) Wind turbine generator reliability: an exploration of the root causes of generator bearing failures. Doctoral dissertation. Durham University, Durham (NC)
20. VDI 3834 (2009) Measurement and evaluation of the mechanical vibration of wind energy turbines and their components—Part 1—Onshore wind energy turbines with gears. International Standard
21. SKF product information high frequency accelerometer CMSS 2100F. SKF Reliability Systems. http://www.skf.com/group/system/SearchResult.html?search=CMSS+2100F. Accessed 12 Aug 2014
22. SKF product information low frequency accelerometer CMSS 2200. SKF Reliability. http://www.skf.com/group/system/SearchResult.html?search=CMSS+2200. Accessed 12 Aug 2014
23. SKF product information datalogger IMx-W. SKF Reliability. http://www.skf.com/group/system/SearchResult.html?search=IMx-W. Accessed 12 Aug 2014
24. Hirschmann (2013) Product information switch RS2-4TX/1FX EEC. https://www.e-catalog.beldensolutions.com/link/57078-24455-49814-49855-351756-34790/en/conf/. Accessed 12 Aug 2014
25. SKF product information CMCP240. SKF Condition Monitoring Custom Products. http://www.stiweb.com/v/vspfiles/downloadables/SKF%20Data%20Sheets/cmcp240.pdf. Accessed 12 Aug 2014
26. Azevedo HDM (2015) Um método para identificação de falhas em componentes e subcomponentes de turbinas eólicas através de monitoramento de condição baseado em vibração. Master dissertation. Federal University of Pernambuco, Recife (PE)
27. Wowk V (1991) Machinery vibration measurement and analysis, 1st edn. McGraw-Hill, USA
28. Miao Q, Cong L, Pecht M (2011) Identification of multiple characteristic components with high accuracy and revolution using the zoom interpolated discrete Fourier transform. Meas Sci Technol. doi:10.1088/0957-0233/22/5/055701
29. Jayaswal P, Agrawal B (2011) New trends in wind turbine condition monitoring system. Int J Emerg Trends Eng Dev 3(1):133–148
30. Miller AJ (1999) A new wavelet basis for the decomposition of gear motion error signals and its application to gearbox diagnostics. Doctoral dissertation. The Pennsylvania State University, Pennsylvania (USA)
31. Cheng J, Yang Y, Yu D (2010) The envelope order spectrum based on generalized demodulation time–frequency analysis and its application to gear fault diagnosis. Mech Syst Signal Process 24(2):508–521. doi:10.1016/j.ymssp.2009.07.003
32. Tandon N, Nakra BC (1992) Comparison of vibration and acoustic measurement techniques for the condition monitoring of rolling element bearings. Tribol Int 25(3):205–512. doi:10.1016/0301-679X(92)90050-W
33. Mcfadden PD (1986) Detecting fatigue cracks in gears by amplitude and phase demodulation of the meshing vibration. J Vib Acoust Stress Reliab Des 108(2):165–170. doi:10.1115/1.3269317
34. Machinery Lubrication Magazine (2015) One vibration analysis expert shares his views about the importance of oil analysis. http://www.machinerylubrication.com/Read/36/oil-analysis-vibes. Accessed 01 Sep 2016